THE SPECTROSCOPY OF QUANTUM DOT ARRAYS

Arrays of nanometer potential wells, fabricated at semiconductor interfaces, exhibit infrared absorption lines reminiscent of atoms, molecules and even crystal lattices.

Detlef Heitmann and Jörg P. Kotthaus

For three decades individual transistors in integrated semiconductor circuits have been getting smaller and smaller. Soon they will be approaching the 100-nanometer regime, where the classical description of diffusive electron motion breaks down and quantum concepts become important, bringing about fundamental changes in electronic and optical properties. Already in the widely used silicon MOSFET transistors, the interface between the semiconductor and the oxide layer serves as a potential well less than 10 nm wide. While electrons remain free to wander in the plane of the interface, their motion in the perpendicular direction is quantized by this very narrow well. Such two-dimensional electron systems, best realized in high-mobility modulation-doped semiconductor heterostructures, have been found over the years to exhibit new and quite unexpected quantum phenomena, like the integral and fractional quantum Hall effects.

The richness of new physics discovered in two-dimensional semiconductor systems, as well as the progress in technologies for lateral patterning of such structures, has challenged many researchers to fabricate and study systems of still lower electronic dimensionality: quantum wires and quantum dots.[1] (See the February 1990 special issue of PHYSICS TODAY, the October 1992 article by Leroy Chang and Leo Esaki, and the January 1993 article by Marc Kastner.) Imposing ultrafine lateral confinement at length scales of about 100 nm on an originally two-dimensional system will also quantize the electron motion in the lateral directions. If the original two-dimensional system defines the xy plane, a narrow confining potential acting in the x direction produces a quantum wire. Finally we come to the quantum dot, an artifical atom with a totally discrete energy spectrum, created by confining potentials in both the x and y directions.[2-6]

An array of such quantum dots may be envisioned as a periodic potential landscape filled with electrons up to some Fermi level. (See figure 1a.) Because the orthogonal z confinement is usually much stronger than the in-plane confinement, the electron distribution in a quantum dot is pancake-like rather than spherical. When more electrons are injected into the lateral confining potential, they eventually spill over to create a topologically complementary structure of so-called antidots, which can be envisioned as an array of island voids rising out of a two-dimensional electron sea.[7-9] (See figure 1b.)

Just as with real atoms, one expects to obtain information about the quantum-confined energy levels in these low-dimensional systems by optical studies of the electronic transitions. It turns out that the dynamic response of quantum dots exhibits a complex interplay of atom-like single-particle behavior and collective many-body effects.

Most of the experiments on low-dimensional electron systems are done with modulation-doped AlGaAs–GaAs heterostructures, because of their superior electron mobility. Let us recall some relevant parameters of gallium arsenide. Its dielectric constant ϵ is 12, and the effective mass m^* of the conduction electrons is only 7% of the free-electron mass m_0. Thus the effective Rydberg energy R_y^*, given by $m^* R_y/(m_0 \epsilon^2)$, is about 6 *milli*-electron-volts, and

Detlef Heitmann is a professor at the University of Hamburg's Institute for Applied Physics. **Jörg Kotthaus** is a professor of physics at the Ludwig–Maximillians University of Munich.

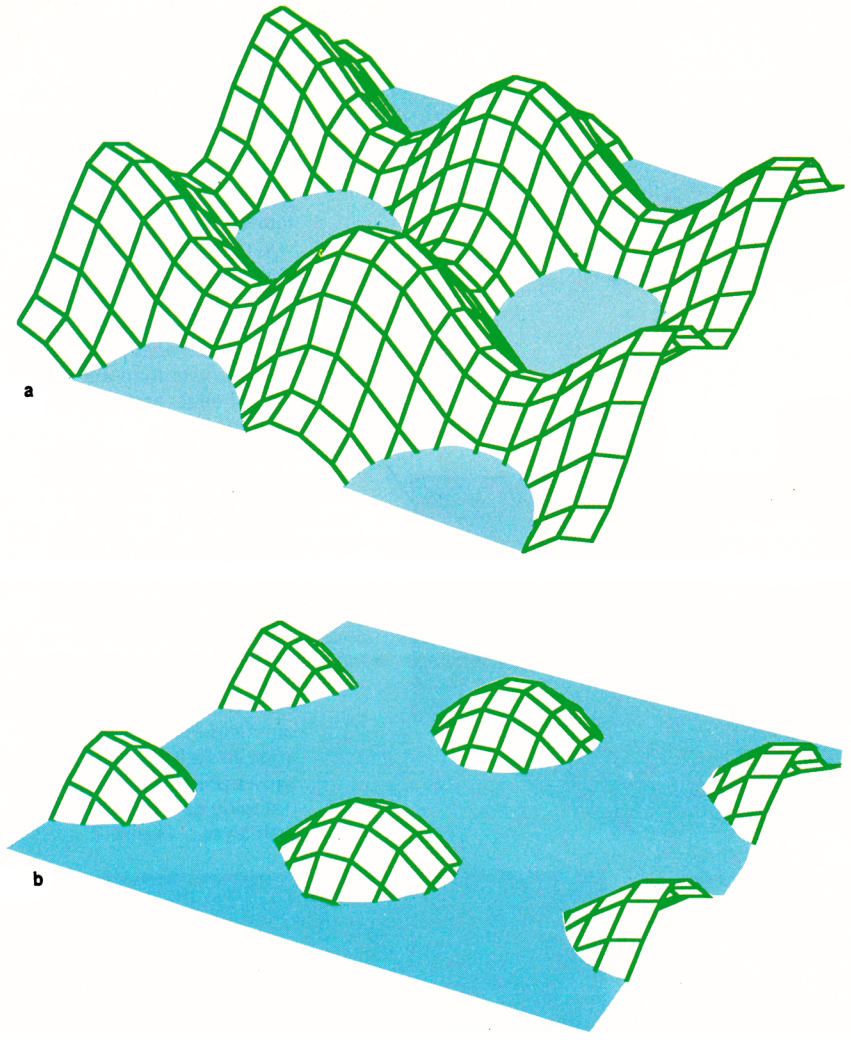

Topology of arrays of quantum dots and antidots in a periodic potential landscape. **a:** When the level of the Fermi electron sea (blue) is low, the electrons are confined in quantum dots looking like isolated mountain lakes. **b:** When the Fermi level is raised, the electrons eventually spill over into a connected sea studded with quantum antidots (green). **Figure 1**

the effective Bohr radius a^*, given by $\epsilon a_0 m_0/m^*$, is 10 nanometers. That's almost 200 times the Bohr radius a_0 of the hydrogen atom.

In a rectangular, infinitely deep GaAs potential well of width w, the energy difference ΔE between the first and second quantized levels is given by $R_y{}^*(\pi a^*/w)^2(2^2 - 1^2)$. If, for example, the well is 50 nm wide, that comes to 6 meV. Thus the very small effective electron mass in GaAs lets one observe quantum effects beyond the broadening mechanisms in systems with dimensions accessible by modern lithographic techniques. Even higher quantization energies can be achieved in narrow-bandgap semiconductors with correspondingly smaller effective masses. In indium–antimony devices,[3] for example, the effective electron mass is only $0.014m_0$. But with InSb the challenge is to prepare devices of sufficiently high electron mobility.

The spectroscopic range for optical studies of atom-like transitions between quantized levels in quantum dots is the far infrared. At the relevant far-infrared wavelengths, the semiconducting materials are quite transparent at low temperatures in the absence of conduction electrons. We measure the small amount of absorption caused by the excitation of electron states in the quantum dots by comparing infrared transmission through an array with and without conducting electrons in the dots.

At near-infrared and visible wavelengths, studies of such nanostructures involve transitions between valence band and conduction band states, and they are further complicated by electron–hole interactions. (See the article by Arto Nurmikko and Aron Pinczuk on page 24 of this special issue.)

Fabrication of quantum dots

Two examples of quantum dot structures are sketched in figure 2a and 2b. Both are fabricated from modulation-doped AlGaAs–GaAs heterostructures. The dopant is implanted in part of the AlGaAs layer, and the electrons are strongly confined in the GaAs at the interface, thus forming a two-dimensional electron system. A periodic array of photoresist dots defined by holographic lithography[1] serves as the mask for further processing. The "deep-mesa-etched" quantum dots of figure 2a are made by dry-etching deep grooves all the way into the active GaAs. The etching leaves behind a landscape of cylindrical mesas, each about 500 nm in diameter. The effective diameter w of the electronic system (typically 100 nm) is significantly smaller than this geometrical size, because some of the electrons from the doped AlGaAs region are trapped by surface states at the open etched sidewalls, where they help confine the conduction electrons to the inner reaches of the dot. Thus the boundary of the confining potential does not coincide with the physical sidewalls of the dot; it is formed electrostatically by the do-

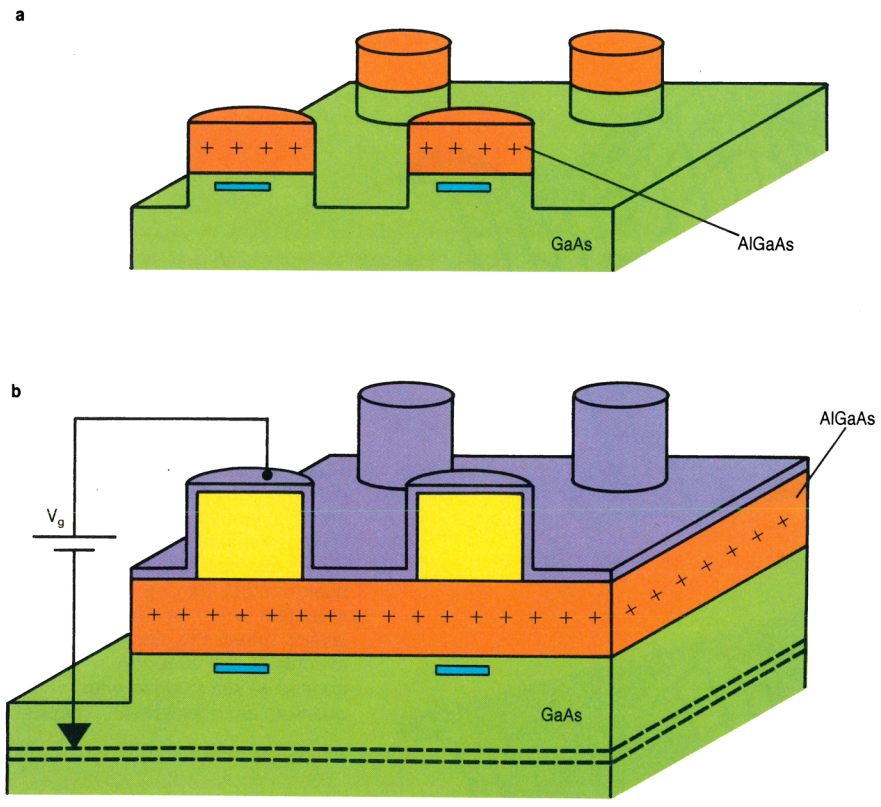

Two ways of making quantum dot arrays at an interface between GaAs (green) and n-doped AlGaAs (red). Both start with an array of photoresist dots serving as a mask. "Deep-mesa-etched" quantum dots (**a**) are fabricated by etching all the way down into the GaAs, leaving mesas typically 500 nm wide. The potential wells (blue) in which the electrons are trapped near the interface are narrower than the mesas. A field-effect array (**b**) is made by depositing a semitransparent metal gate (purple) on the photoresist mask (yellow). Voltage applied between the gate and a semitransparent contact layer (between dashed lines) in the GaAs concentrates the interface electrons into potential wells where the gate is farthest away. A scanning electron micrograph (**c**, below) of a field-effect quantum dot array in an InSb structure[3] shows photoresist dots 100 nm wide covered by a metal gate layer. **Figure 2**

nor ions and fixed surface charges surrounding the dot.

Figure 2b shows a semitransparent metal gate deposited on the photoresist mask to form a textured capacitor. A negative voltage applied at the gate relative to a thin semitransparent contact layer electrically coupled to the active electron system above it causes the depletion of conduction electrons wherever the gate is closest to the AlGaAs–GaAs interface. Thus a device is created in which one can vary the Fermi level by tuning the voltage. As the electronic sea level falls, the homogeneous two-dimensional electron system becomes an antidot array and finally an array of quantum dots, as we saw in figure 1. Figure 2c is an electron micrograph of a tunable array of field-effect quantum dots on InSb with a period of 250 nm between adjacent dots.

Far-infrared spectroscopy

Far-infrared radiation can directly induce optical transitions between the meV energy levels confined in the quantum dot. To achieve a detectable signal requires dot arrays with active sample areas on the order of 10 mm^2. Fabricating such a surface, with its 10^8 nearly identical quantum dots, poses quite a challenge. Typically such spectroscopic experiments are carried out at liquid helium temperatures to eliminate thermal broadening. Waveguides couple the radiation from a suitable source, either a Fourier-transform spectrometer or a far-infrared laser, to the sample, and a cryogenic detector measures the transmitted radiation.

The experimenter often applies a magnetic field normal to the interface. One can exploit the interplay between electronic and magnetic confinement very effectively to characterize lengths, energies and interactions in quantum dots. In a magnetic field B the cyclotron energy $\hbar eB/m^*$ of the conduction electrons becomes comparable to the confining energy in the quantum dot. (In GaAs at

c

1 tesla, the cyclotron energy is 1.8 meV.) Equivalently, the radius of the cyclotron orbit becomes comparable to the typical lateral confinement length.

Figure 3a shows the relative change with frequency of far-infrared transmission through a square quantum dot array on GaAs with a spatial period of 500 nm, with and without an applied magnetic field. The gate voltage is chosen so that each dot contains about 50 electrons. This occupancy level can be directly deduced from the strength of the transmission signal integrated over frequency. The transmission coefficient is normalized to the transmission when the gate voltage is tuned to keep the dots empty.

In the absence of an external magnetic field, the spectrum (blue curve in figure 3a) shows only one absorption resonance. That's somewhat surprising for so

many electrons in each dot. The resonance occurs at a wavenumber of about 30 cm^{-1}, corresponding to a wavelength of 330 microns in the far infrared and a photon energy of 3.7 meV. If one imposes a 1.4-tesla magnetic field normal to the array plane, the resonance splits in two (red curve). Figure 3b shows how this splitting emerges with increasing magnetic field. While the lower branch decreases in frequency with increasing field, the upper branch increases toward the cyclotron resonance frequency. Surprisingly, one finds in such experiments that neither this dispersive splitting nor the absolute frequencies depend strongly on the number of electrons per dot. That's quite different from what we are used to in ordinary atoms. This lack of sensitivity to electron population turns out to be a characteristic signature of parabolic confining potentials.

Dipole excitations

The explanation of the experimentally observed spectra is intimately connected with the shape of the confining potential. Model calculations show that the bare external confining potential for electrons in a field-effect quantum dot has a nearly parabolic shape.[10] This shape can be understood from the charge distributions indicated in figure 2. The strong confinement of the conduction electrons along the growth direction of the heterostructure restricts their motion to the xy plane of the interface. Fixed donor charges in the AlGaAs layer, charged surface states and the spatially modulated electrostatic field in the gated structure define the equilibrium position of the conduction electrons in the center of the dot. Displacing these electrons in the xy plane produces a restoring force approximately linear in the displacement. Consequently the confining potential $V(x,y)$ is $\frac{1}{2}m^*\Omega_0^2(x^2+y^2)$. That is to say, it is parabolic, with a characteristic frequency Ω_0 determined by the electrostatic environment.

The energy spectrum for a single electron confined by such a parabolic potential in the presence of a magnetic field was already calculated in 1928 by Vladimir Fock at Göttingen.[11] The dipole-allowed transitions in this spectrum have energies[3]

$$\Delta E^{\pm} = \sqrt{\hbar^2\Omega_0^2 + (\hbar\omega_c/2)^2} \pm \hbar\omega_c/2 \qquad (1)$$

where ω_c is the cyclotron frequency for a given magnetic field. This equation describes well the observed dispersion of the split absorption resonance with increasing magnetic field, shown in figure 3b.

But there is more than one electron in a quantum dot. For a small number of electrons per dot it is possible to calculate many-electron wavefunctions and energy states.[12] The many-body spectrum at zero magnetic field is then governed by two characteristic energies: the quantum confinement energy E_q and the Coulomb energy E_C. For the simplest case of two parabolically confined electrons, which one might call the "helium" of the quantum dot atoms, these parameters may be expressed in terms of l_0, the confinement length of the harmonic oscillator, as $E_q = \hbar^2/(m^*l_0^2)$, and $E_C = e^2/(4\pi\epsilon\epsilon_0 l_0)$, where l_0 is given by $\sqrt{\hbar/m^*\Omega_0}$. The energy ratio E_C/E_q is simply l_0/a^*.

With increasing l_0 both energies decrease, but the Coulomb energy increasingly dominates over the confinement energy. Figure 4 compares two different calculations of the energy spectrum for two electrons in a parabolic well with $l_0 = a^*$. The spectrum on the left assumes the two electrons to be independent of each other; the right-hand spectrum includes their mutual interaction. We see that the interaction increases the ground state energy of the two-electron system. This "Coulomb charging energy" is the cost for squeezing the second

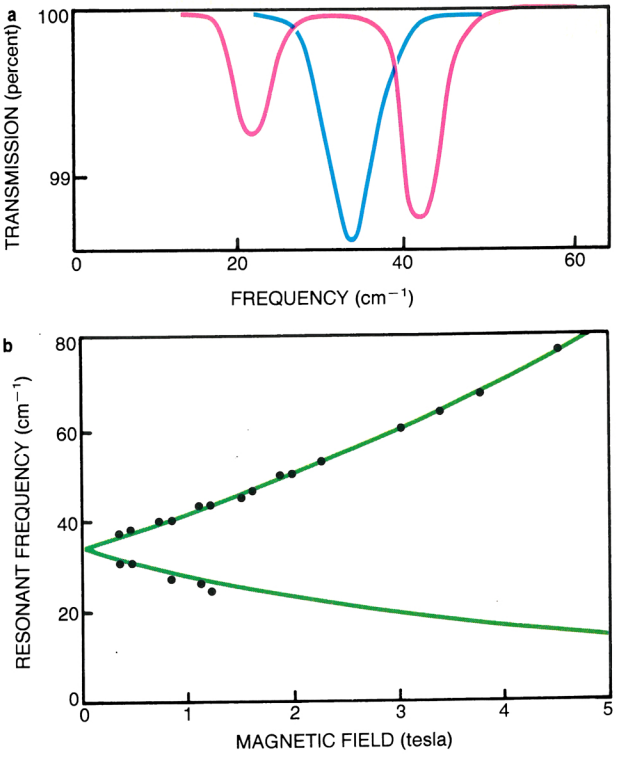

Far-infrared resonance freqencies due to electronic excitations in a quantum dot array on GaAs. **a:** Transmission coefficient plotted against wavenumber shows a single absorption resonance in the absence of an applied magnetic field (blue curve). In a 1.4-tesla field (red curve) the resonance has split in two. **b:** The dispersion of these two resonances widens with increasing applied magnetic field. (Adapted from ref. 6.) **Figure 3**

electron into the quantum dot. The electron–electron interaction also lifts some of the degeneracies of the one-electron energy levels, giving rise to a complex spectrum with singlet and triplet states.

A unique spectroscopic property of parabolically confined electrons is that the dipole-allowed transitions for two interacting electrons have exactly the same energy, $\hbar\Omega_0$, as the one-electron transition. Moreover, this result also holds for an arbitrary number of electrons in the dot. The Hamiltonian for an interacting, parabolically confined many-electron system is separable into two parts describing, respectively, the center-of-mass motion of the whole electron system and the relative internal motions of the electrons.[13] Furthermore, because the far-infrared wavelengths in the experiments are ten thousand times larger than the dot diameter, the dipole approximation is very well fulfilled and the exciting electric fields couple only to the center-of-mass motion. Thus the optical dipole response of a quantum dot with parabolic confinement, in the absence of a magnetic field, represents a rigid collective center-of-mass excitation at Ω_0, the frequency of the bare external potential. It is independent of the number of electrons confined in the dot and their Coulomb interactions. This result is a generalization of the famous Kohn theorem: In 1961 Walter Kohn, at the University of California at San Diego, showed that the cyclotron resonance frequency in a translationally invariant system

is not affected by electron–electron interactions.[14]

Because the far-infrared response of the electron system in a quantum dot reflects primarily the rigid center-of mass motion, it is appealing to approach these excitations also by way of a model of classical collective modes. Equation 1, the dispersion equation one gets from quantum mechanics, can also be derived classically as describing a plasma oscillation, or a depolarization mode, in which, in the absence of a magnetic field, a disk of conduction electrons moves back and forth rigidly with respect to the fixed donor ions.[15] As the resonance splits and separates with increasing magnetic field, the cyclotron orbit eventually becomes much smaller than the dot diameter. Then the classical model describes the two resonant frequencies as follows: The high-frequency mode is a magnetoplasma oscillation that approaches the cyclotron resonance. In this mode all electrons orbit coherently around individual centers at the cyclotron frequency and hardly feel the confinement of the dot potential. The lower-frequency mode reflects a collective motion of the centers of all the cyclotron orbits around the center of the dot. In this mode each cyclotron-orbit center drifts around the center of the dot under the joint influence of the confining electrostatic field E and the imposed magnetic field B, with a drift velocity v_d given by E/B. The corresponding frequency at large magnetic fields, $v_d/r = \Omega_0^2/\omega_c$, thus decreases as $1/B$. For a square-well dot potential this mode becomes localized at the edge of the dot in a strong magnetic field. Therefore it is often called an edge magnetoplasmon.

The generalized Kohn theorem clarifies why optical spectroscopy on parabolically confined quantum dots is much less specific than it is on ordinary atoms. It also indicates that a nonparabolic potential should make it possible to access relative electron motion spectroscopically in quantum dots. Additional, weaker fine structure has been spectroscopically observed in quantum dot arrays, manifesting the excitation of internal motions.[4,6] But because such fine structure has thus far only been observed in quantum dots larger than a^*, the character of these additional excitations is still predominantly collective. In spectroscopic studies on quantum wires one also finds that a single collective center-of-mass mode dominates the far-infrared response.[1,16,17]

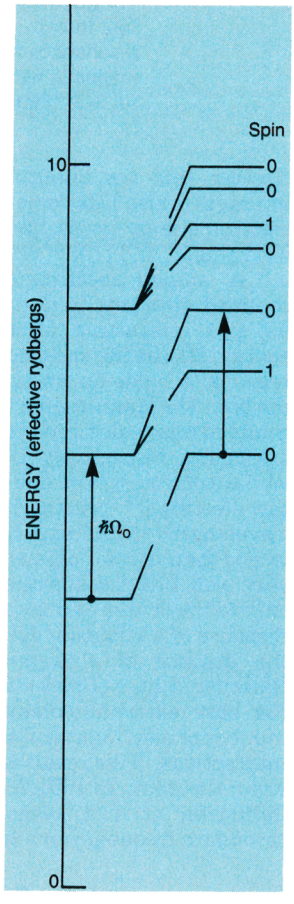

Calculated energy spectra for two independent electrons (left) and two interacting electrons (right) confined in the parabolic potential of a quantum dot whose harmonic oscillator radius equals its effective Bohr radius. Coupling raises and splits the degenerate independent-electron levels into sublevels characterized (and labeled) by total spin (1 or 0). But the energy $\hbar\Omega_0$ of the dipole-allowed transition (arrows) remains the same, unaffected by the interaction between electrons. (Adapted from ref. 12.) **Figure 4**

Charging with single electrons

The generalized Kohn theorem tells us that for parabolic confinement one cannot determine the number of electrons in a quantum dot atom from its resonant frequency. But far-infrared spectroscopy gives us not only the resonant frequency but also the absorption strength, which is a measure of the electron population per dot. For a parabolic potential at $B = 0$ all absorption occurs at a single resonant frequency. It follows that absorption strength increases in direct proportion to the number of electrons in the quantum dot. A careful measurement[6] of absorption strength versus gate voltage in a field-effect quantum dot array with a spatial periodicity of 200 nm is displayed in figure 5. Surprisingly, one finds that the absorption at low electron occupancy increases step-wise with gate voltage. Starting with a single electron in each dot, the electron population increases by one with each step. This behavior of the infrared absorption strength shows that most of the 10^8 dots in the array change their charge by one electron at just about the same gate voltage. At first glance that's rather puzzling.

The cause of this well-defined charging behavior lies in the relatively large Coulomb charging energy required to squeeze an additional electron into a quantum dot. (Recall figure 4.) One gets a rough estimate of the Coulomb charging energy classically from what might be called the "capacitance" of the dot. Take the simple model of a parallel-plate capacitor, where one plate is formed by the quantum dot electron disk with a diameter defined by the extent of the wavefunction in a harmonic oscillator. That diameter is 54 nm for the experiment[6] whose results are shown in figure 5. (Note that this "capacitance" varies with increasing charge.) Then, taking the distance to both the front gate and the back contact layer into account, one gets a capacitance C of 5×10^{-18} farads and a related charging energy, given by $e^2/2C$, of about 15 meV. This energy is significantly larger than the thermal energy kT. It ensures that Coulomb charging effects are smeared out neither by temperature nor by unavoidable potential fluctuations.

Experimentally one can obtain a more reliable value of the Coulomb charging energy from the gate voltage interval ΔV_g it takes to add one additional electron to each dot.[6] In figure 5 it takes 30 mV to increase the dot occupancy from two to three electrons. The capacitance equals $e/\Delta V_g$, so that the charging energy $e^2/2C$ equals $e\Delta V_g/2$, or 15 meV, which is just what the geometrical estimate gave. The observation of such single-electron charging phenomena, now widely studied in small metallic and semiconductor systems,[18] assures us that present fabrication technologies can produce extremely uniform arrays of quantum dots. That capability opens a wide field for the study of detailed quantum effects and interactions in controlled few-electron systems.

Artificial molecules and solids

Having prepared uniform arrays of artificial atoms, it is

natural that one starts to look for quasimolecular and solid-like interaction phenomena between quantum dots. The voltage-tunable confining potentials that let one add single electrons to quantum dots in large arrays also make it possible to fabricate artificial quantum dot "solids." To accomplish that, one electrostatically controls the coupling between adjacent dots by adjusting the Fermi sea level sketched in figure 1. Raising the Fermi energy in a dot array will eventually open narrow conducting channels where the dot perimeters touch. In practice this is done by raising the gate voltage in a suitable field-effect dot array. Once the dots become electrically connected, new lines appear in the infrared transmission spectra that manifest the coupling in a characteristic manner quite analogous to what we know well from atoms interacting in molecules or solids.

The magnetic dispersion of the infrared resonances in such an array is shown in figure 6 for dots that are weakly coupled by narrow conducting channels in the borderline case between dots and antidots.[5] (See the inset.) In this case two more spectral lines are observed in addition to the characteristic quantum dot modes. The new lowest-frequency mode can be understood as representing the center-of-mass motion of the electrons guided by the $\mathbf{E}\times\mathbf{B}$ drift of the cyclotron orbits between two adjacent quantum dots. It is a characteristic edge-magnetoplasmon-like excitation of a diatomic quantum dot molecule, with charge moving ballistically back and forth through the narrow constriction between two adjacent dots. Other possible quasimolecular modes experience stronger damping because they involve passage through two or more narrow channels and are therefore no longer discernible in the experimental spectra.

As we see in figure 6, the high-frequency single-dot branch splits in two when the magnetic field becomes strong enough to render the cyclotron orbits small enough to fit into the narrow channels beween adjacent dots. The new uppermost branch can be identified as a two-dimensional bulk-like plasmon mode with its wavelength determined by the period of the dot array. Thus it is analogous to a phonon mode of the quantum dot solid, directly reflecting the long-range coupling in the array structure when the Fermi level is high enough for narrow channels to form between dots.

It might seem surprising that the center-of-mass mode description, which is strictly valid only for parabolic confining potentials, remains useful for the molecular excitation discussed above, where the potential has certainly acquired substantial nonparabolic terms. The reason is that the far-infrared light uniformly irradiating the array couples best to the coherent motion of the conduction electrons with respect to the background charge, even if the bare confining potential becomes rather nonparabolic. This becomes even more apparent at higher Fermi levels, when dots, or antidots, become strongly coupled.

Collective motion among the antidots

Another type of artificial lateral superlattice is the antidot array. As sketched in figure 1b, such an array consists of periodically placed repulsive potentials in the plane of a two-dimensional electron system. One can generate arrays of antidots electrostatically with suitably patterned gates. The periodic arrays can also be made with focused ion beams or by etching geometric holes into the heterostructure.

The magnetic dispersion of far-infrared excitation frequencies in such an antidot array is shown in figure 7a. The array was prepared at the Max Planck Institute in Stuttgart by etching deep holes into a modulation-doped

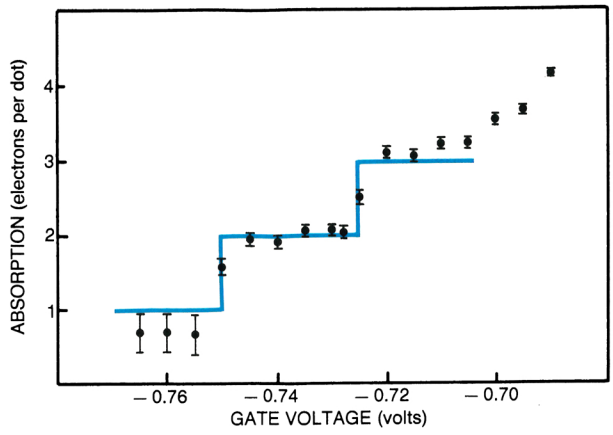

Steplike increase of far-infrared absorption (integrated over frequency) with changing gate voltage in a square field-effect array of 10^8 quantum dots shows that the dots increase their occupancies almost simultaneously, one electron at a time. (Adapted from ref. 6.) **Figure 5**

GaInAs–AlInAs single quantum well.[8] Because of the relatively small lateral electron depletion at the etched sidewalls of the GaInAs region, one can create holes of very small electrical radius. The two infrared resonances in figure 7a have a magnetic field dispersion that is distinctly different from what one gets with quantum dots. The difference can be understand as follows: At high B the dispersion of both branches in figure 7a resembles the excitation spectrum we have seen for quantum dots. The higher-frequency mode at high magnetic field intensities, where it approaches the cyclotron frequency, represents a cyclotron-like motion in the region between the antidots. At small B this mode shows a weak but distinct negative dispersion; that is to say, the resonant frequency *decreases* with increasing B. This is a signature that the mode represents, at small B, a kind of one-dimensional plasmon that propagates along the charged stripes between the geometrical holes with a wavelength given by the periodicity of the array.[17]

The lower-frequency branch eventually falls with increasing B, as it does in dot arrays. This branch represents an edge magnetoplasmon mode. In dot arrays, the individual electrons of this collective mode execute skipping orbits along the *inner* boundary of the dot. (See the red trajectory in the inset of figure 6.) For antidots, however, the individual electrons within the collective excitation perform skipping orbits *around* the hole. Because the electron orbits grow with decreasing B, the electrons can eventually perform classical cyclotron-like orbits around the geometrical hole. Therefore, in contrast to what one observes for dots, the edge magnetoplasmon resonance of the low-frequency branch changes its character as B approaches zero: The frequency approaches the *decreasing* cyclotron frequency. The collective edge magnetoplasmon excitation at large B has gradually gone over to a classical cyclotron excitation. For the sample characterized in figure 7a, the classical cyclotron radius comes to equal the radius of the holes at a field strength of about 1 tesla. That is indeed where the turnover occurs. Experiments verify that the dispersion turns over at higher B when one uses smaller holes, as this model predicts.

Antidot arrays also exhibit intriguing magnetoresist-

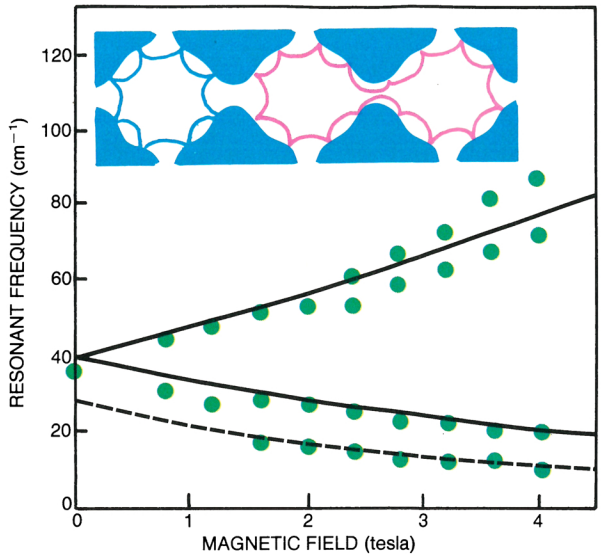

Four dispersion modes, instead of the usual two (solid curves), appear in a plot of resonant infrared absorption frequency against applied magnetic field when the quantum dots in the absorbing array are coupled to their neighbors by weak electrical channels, as indicated in the inset. The lowest of the four modes (dashed line) can be interpreted as a quasimolecular excitation involving adjacent pairs of quantum dots, as indicated by the red trajectory in the inset. The highest-frequency mode is a phonon-like collective excitation of the whole array behaving like a two-dimensional solid. The spacing between quantum dots in the square lattice array is 450 nm, and each dot houses about 80 electrons. (Adapted from ref. 5.) **Figure 6**

ance properties that have been successfully explained by classical ballistic trajectory models.[7,9] Whenever the classical cyclotron diameter approaches the period of the antidot array or multiples thereof, the magnetoresistance exhibits "commensurability oscillations" that arise from an interplay between chaotic and stationary trajectories. The success of such classical models has triggered an attempt to use the same kind of trajectory calculation to model the high-frequency electronic modes in more complex structures such as arrays of coupled dots.[9] In such a calculation one uses the classical equations of motion to determine the trajectories of a single electron moving ballistically at constant Fermi energy in the landscape of the periodic potential and an imposed magnetic field. Using randomly chosen initial coordinates and velocities, one computes large sets of trajectories. The high-frequency response is then calculated by Fourier analysis of the velocity component along the high-frequency electric field. A phenomenological damping parameter simulates the destruction of deterministic ballistic motion by random scatterers.

For a single electron confined in a parabolic quantum dot such a classical model yields the same resonance frequencies as the quantum mechanical model from which one gets equation 1. The results of such a calculation for an antidot array are displayed in figure 7b. The resonant frequencies calculated with a model potential similar to the screened periodic potential of the experimental devices come out *lower* than the observed frequencies. That's because the collective center-of-mass motion in the experiments tests the bare, unscreened potential. Because the single-electron trajectory model cannot include such collective effects, it reflects the softer, screened potential. The one-particle approach also fails to describe the negative B dispersion of the high-frequency resonance branch. Nonetheless this simple trajectory model does reproduce most features of the observed magnetic field dispersion for the complex excitations in an antidot array.

Dipolar coupling

An additional, distinctly different coupling mechanism can arise from the dipolar Coulomb interaction between electrically isolated quantum dots. This mechanism is most easily envisioned by considering a single electron bound in the plane of a quantum dot by a fixed positive charge located above that plane. A displacement of the electron from equilibrium induces a dipole moment in the plane, which in turn can polarize an adjacent quantum dot. Such classical dipolar interdot interaction has been considered for different quantum dot geometries. Under sufficiently favorable conditions it is predicted to give rise to a ferroelectric or antiferroelectric phase transition.[19]

These conditions for a so-called polarization catastrophe may not be realizable for some time to come. They require the binding of very small electron populations into quantum dots with highly anisotropic confining potentials. Nonetheless they pose a very challenging experimental problem, for two reasons. One is that such ordering in quantum dot arrays would make it possible to study symmetry-breaking phase transitions in artificial two-dimensional solid-like systems. The other is that strong dipolar coupling between adjacent dots may eventually open a route to the use of quantum dot arrays for computational purposes. One promising scheme, recently put forward by Craig Lent and coworkers at Notre Dame University, is based on cellular automata. It employs the dipolar coupling between quantum dots to transfer information between adjacent cells without connecting wires.

Such dipolar coupling can be demonstrated even before the onset of any phase transition by studying the far-infrared modes. A recent experiment at the University of Munich on classical (as distinguished from quantum) circular dots placed on a rectangular lattice demonstrated how the dipolar coupling manifests itself in the high-frequency modes.[20] Instead of the mode degeneracy that is characteristic of a single circular dot in the absence of a magnetic field (as shown in figure 4) one finds two modes when circular dots are placed on a rectangular lattice so that their spacing is much smaller in one direction than in the other. This splitting provides a direct measure of the relative strength of the dipolar coupling along the two axes of the rectangular lattice. Splitting and softening of the low-frequency mode is thus also a signature of dipolar interaction in quantum dots. It can be used as a measure of this interaction even before a symmetry-breaking phase transition occurs. At the phase transition, where the dynamic polarization becomes static, the low-frequency infrared mode will go to zero frequency, reflecting the absence of a net restoring force for the electron.

What's ahead?

One of the surprising results from the investigation of quantum dot arrays has been that many aspects of spectroscopic and transport phenomena can be described classically—this despite the fact that quantum dots contain few electrons and confinement lengths are comparable to their de Broglie wavelengths. In large part this is due to the parabolic shape of the bare confining potentials fabricated thus far. Such confining potentials are dominated by charges relatively far from the confined electrons. Thus the far-infrared spectra reflect most prominently their harmonic-oscillator-like collective motion.

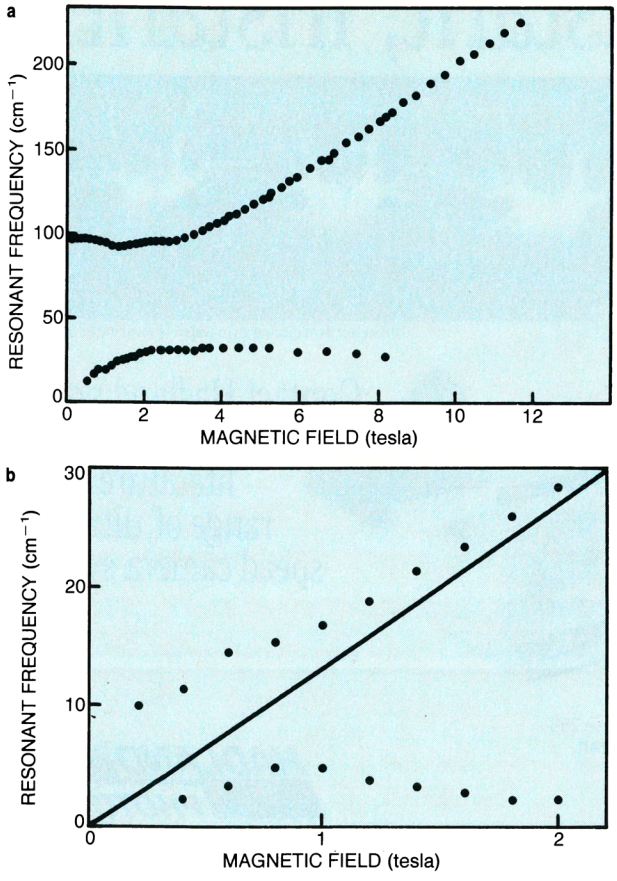

For antidot arrays, the observed dispersion of resonant absorption frequency with increasing applied magnetic field (**a**) is quite different from what one finds with ordinary quantum dot arrays (as shown, for example, in figure 3b). The antidot array with which these data were taken has a period of 300 nm and a hole diameter of 200 nm; it was made by deep mesa etching on a GaInAs–AlInAs heterostructure. (Adapted from ref. 8.) The predicted spectral response (**b**) of a single ballistically moving electron at a Fermi energy of 25 meV in an antidot potential 40 mV deep is calculated from a simple classical trajectory model. The diagonal line indicates the cyclotron frequency. (Adapted from ref. 9.) **Figure 7**

Relative motion among the electrons, by contrast, will become more easily visible when the confining potentials become nonparabolic or when materials with nonparabolic band structure come into use. One can achieve a nonparabolic potential shape by bringing the charges that control the confinement closer to the confined electrons. Though successful attempts in that direction have already been made, the nanolithographic technologies still need further refinement. One ingenious, highly promising route to tightly confined quantum dots uses patterned substrates combined with multilayer epitaxy to grow very small quantum wires and dots. With such an approach Eli Kapon and colleagues at Bellcore demonstrated the first successful operation of a quantum wire laser.[21] It now appears possible to use similar techniques to fabricate quantum dots only a few tens of nanometers across, with controllable size, confining potential and electron population. Once such systems are realized we can expect to observe more specific electronic spectra that clearly exhibit spectral differences between quantum dot "hydrogen" and "helium."

It remains an open question whether quantum dots will ever be useful in the sense of forming the backbone for some future nanoelectronic architecture based on cellular automata or neural networks. Such developments appear to be possible, but it will probably be many years before our present concepts are confronted with the practical tests of realizability, technological stability and tolerance. In the shorter run, studies of quantum dots and the structures that can be built with them are likely to produce important new insights into fundamental physics issues such as the effects of spin, single-electron charging, ballistic and chaotic motion, commensurability and fractal dimensionality on the electronic properties of these artificial atom-like structures.

We thank Claus Dahl and Ulrich Merkt for very helpful comments on the manuscript, and many colleagues in the field of nanostructures for cooperation and stimulating discussions.

References

1. For an introduction to semiconductor nanostructures see M. Reed, W. Kirk, eds., *Nanostructures and Mesoscopic Systems*, Academic, San Diego (1991); R. K. Williardson, A. C. Beer, E. R. Weber, eds., *Nanostructured Systems*, Semiconductors and Semimetals, vol. 35, Academic, San Diego (1992).
2. M. A. Reed, J. N. Randall, R. J. Aggarwal, R. J. Matyi, T. M. Moore, A. E. Wetsel, Phys. Rev. Lett. **60**, 535 (1988). W. Hansen, T. P. Smith III, K. Y. Lee, J. A. Brum, C. M. Knoedler, J. M. Hong, D. P. Kern, Phys. Rev. Lett. **62**, 2168 (1989).
3. C. Sikorski, U. Merkt, Phys. Rev. Lett. **62**, 2164 (1989).
4. T. Demel, D. Heitmann, P. Grambow, K. Ploog, Phys. Rev. Lett. **64**, 788 (1990).
5. A. Lorke, J. P. Kotthaus, K. Ploog, Phys. Rev. Lett. **64**, 2559 (1990).
6. B. Meurer, D. Heitmann, K. Ploog, Phys. Rev. Lett. **68**, 1371 (1992).
7. K. Ensslin, P. M. Petroff, Phys. Rev. B **41**, 12307 (1990). D. Weiss, M. L. Roukes, A. Menschig, P. Grambow, K. von Klitzing, G. Weimann, Phys. Rev. Lett. **66**, 2790 (1991). R. Fleischmann, T. Geisel, G. R. Ketzmerick, Phys. Rev. Lett. **68**, 1367 (1992).
8. K. Kern, D. Heitmann, P. Grambow, Y. H. Zhang, K. Ploog, Phys. Rev. Lett. **66**, 1618 (1991).
9. A. Lorke, Surf. Sci. **263**, 307 (1992).
10. A. Kumar, S. E. Laux, F. Stern, Phys. Rev. B **42**, 5166 (1990).
11. V. Fock, Z. Phys. **47**, 446 (1928).
12. G. W. Bryant, Phys. Rev. Lett. **59**, 1140 (1987). D. Pfannkuche, R. R. Gerhardts, Phys. Rev. B **44**, 13132 (1991). M. Wagner, U. Merkt, A. V. Chaplik, Phys. Rev. B **45**, 1951 (1992).
13. L. Brey, N. Johnson, P. Halprin, Phys. Rev. B **40**, 10647 (1989). P. Maksym, T. Chakraborty, Phys. Rev. Lett. **65**, 108 (1990).
14. W. Kohn, Phys. Rev. **123**, 1242 (1961).
15. S. J. Allen Jr, H. L. Störmer, J. C. Hwang, Phys. Rev. B **28**, 4875 (1983). A. L. Fetter, Phys. Rev. B **32**, 7676 (1985); **33**, 5221 (1986).
16. W. Hansen, M. Horst, J. P. Kotthaus, U. Merkt, C. Sikorski, K. Ploog, Phys. Rev. Lett. **58**, 2586 (1987).
17. T. Demel, D. Heitmann, P. Grambow, K. Ploog, Phys. Rev. Lett. **66**, 2657 (1991).
18. For a recent review see H. Grabert, M. H. Devoret, eds., *Single Charge Tunneling*, Plenum, New York (1992).
19. K. Kempa, D. A. Broido, P. Bakshi, Phys. Rev. B **43**, 9343 (1991). A. V. Chaplik, L. Ioriatti, Surf. Sci. **263**, 354 (1992). C. S. Lent, P. D. Tougaw, W. Porod, Appl. Phys. Lett., **62,** 714 (1993).
20. C. Dahl, J. P. Kotthaus, H. Nickel, W. Schlapp, Phys. Rev. B **46**, 15590 (1992).
21. E. Kapon, D. Hwang, R. Bhat, Phys. Rev. Lett. **63**, 430 (1989). ■